Molecular electrometer and binding of cations to phospholipid bilayers

Andrea Catte,* Mykhailo Girych,† Matti Javanainen,‡ Claire Loison, Josef Melcr,§ Markus S. Miettinen,¶ Luca Monticelli,** Jukka Määttä,†† Vasily S. Oganesyan,* O. H. Samuli Ollila,‡‡ Joona Tynkkynen,‡ and Sergey Vilov

Despite the vast amount of experimental and theoretical studies on the binding affinity of cations into phosholipid bilayers, especially the biologically relevant Na^+ and Ca^{2+} ions, there is no consensus in the literature. In this paper, we show that the ion binding affinity can be directly compared between simulations and experiments by using the choline headgroup order parameters according to the 'molecular electrometer' concept. [1]. Our findings strongly support the pre-2000 view that Na^+ and other monovalent ions (except Li^+) do not specifically bind to phosphatidylcholine lipid bilayers with mM concentrations, in contrast to Ca^{2+} and other multivalent ions. Especially the Na^+ binding affinity is overestimated by several molecular dynamics simulation models, leading to an artificially positively charged lipid bilayer and overexagerated structural effects in the headgroups. Qualitatively correct headgroup order parameter response is observed with Ca^{2+} binding in all the tested models, however, none of the them has a sufficient quantitative accuracy to interpret the Ca^{2+}:lipid stoichiometry or the induced atomistic resolution structural changes.

This work has been, and continues to be, progressed and discussed through the blog `nmrlipids.blogspot.fi`*, through which everyone is invited to join the discussion and make contributions. The manuscript will be eventually submitted to an appropriate scientific journal. Everyone who has contributed to the work through the blog will be offered coauthorship. For more details see* `nmrlipids.blogspot.fi`*.*

I. INTRODUCTION

Due to its high physiological importance — nerve cell signalling being the prime example — interaction of cations with phospholipid membranes has been widely studied via theory, simulations, and experiments. It is generally agreed that the relative binding affinities of different ions follow the Hofmeister series [2–10], however, consensus on the quantitative binding affinities is currently lacking. Two extensive reviews covering the field until 1990 [3, 4] demonstrate that until that time it was generally considered that while multivalent cations interact significantly with phospholipid bilayers, for monovalent cations (with the exception of Li^+) the interactions are weak. This conclusion has since been further supported by contemporary studies showing that bilayer properties remain unaltered upon the addition of millimolar concentrations of a monovalent salt [5, 11, 12]. However, since 2000, another view, questioning the weakness of interactions between

phospholipids and monovalent cations and suggesting a much stronger binding especially for Na^+, has emerged [7–10, 13–19].

The pre-2000 view is supported by the experimental findings that (in contrast to significant effects by the presence of Ca^{2+} or other multivalent ions) millimolar concentrations of NaCl have a negligible effect on phospholipid infrared spectra [5], area per molecule [11], dipole potential [20], lipid lateral diffusion [12], and choline head group order parameters [21]. In addition, water sorption isotherms for a POPC/NaCl system and NaCl in pure water are very similar — indicating only weak interaction between ions and lipids [5].

The post-2000 view, which in contrast suggests strong Na^+ binding, rests on experimental and simulational findings. The rotational and translational dynamics of fluorescent probes in lipid bilayers decrease with mM NaCl concentrations [8, 10, 13], and bilayer hardness and area per lipid measured with Atomistic Force Microscopy (AFM) change [15–19]. In addition, atomistic molecular dynamics (MD) simulations commonly predict binding of Na^+ ions to phosahatidyl-choline lipid bilayers, although the strength of the binding depends on the specific model used [13, 14, 22–27]. Upon Na^+ binding, some simulation studies reported a reduction in lipid lateral diffusion, *in agreement with the fluorescent probe measurements [8, 10, 13].* Other simulations showed a reduction in area per lipid in the presence of NaCl, *in agreement with AFM experiments [15–19]; however, the reduction in area was observed at excessively low Na^+ concentrations, compared to observations from scattering experiments [11].* Predictions of electrophoretic mobility in the presence of NaCl yielded positive values, higher than in experiments; however, this could be explained by the behaviour of Cl^- ions [23, 28].

Some observables have been interpreted to favor both the pre- as well as the post-2000 views. For example, while the reduced lateral diffusion of fluorescent probes was interpreted to support the post-2000 view, reduction of lipid diffusion was not observed in noninvasive NMR experiments,

---

* University of East Anglia, Norwich, United Kingdom
† Helsinki Biophysics and Biomembrane Group, Department of Biomedical Engineering and Computational Science, Aalto University, Espoo, Finland
‡ Tampere University of Technology, Tampere, Finland
§ Institute of Organic Chemistry and Biochemistry, Czech Academy of Sciences, Flemingovo nam. 2, 16610 Prague 6, Czech Republic, Charles University in Prague, Faculty of Mathematics and Physics, Ke Karlovu 3, 121 16 Prague 2, Czech Republic
¶ Fachbereich Physik, Freie Universität Berlin, Berlin, Germany
** Institut de Biologie et Chimie des Protéines (IBCP), CNRS UMR 5086, Lyon, France
†† Aalto University, Espoo, Finland
‡‡ **Author to whom correspondence may be addressed. E-mail: samuli.ollila@aalto.fi.**,Department of Neuroscience and Biomedical Engineering, Aalto University, Espoo, Finland

suggesting that fluorescence results arise from Na^+ interactions with probes rather than with lipids [12]. And as the effect of monovalent ions (except Li^+) on the phase transition temperature is small (compared to the effect of multivalent ions), it was initially interpreted as an indication that only multivalent ions and Li^+ specifically bind to phosholipid bilayers [3]; however, more recently such small effect in calorimetric measurements was interpreted to indicate that also Na^+ binds [9, 13]. Finally, in electrophoresis measurements on phosphatidylcholine vesicles, positive zeta potentials can be generally reached only with multivalent ions or Li^+, whereas NaCl increases the (initially negative) zeta potential to only about zero [2, 9, 15, 16, 29]. This lack of significant positive electrophoretic mobility in the presence of NaCl suggested weak binding of Na^+; however, the same data has also been explained by an effect of the Cl^- ions [23, 28].

In the present work we set out to solve the apparent contradictions between the pre-2000 and post-2000 views by directly comparing the headgroup order parameters of hydrocarbon segments α and β (see Fig. 1) between simulations and experiments as a function of cation concentration. According to the 'molecular electrometer' concept, changes in order parameters of the α and β carbons in the phospholipid head group can be used to measure the ion affinity to the phophatidylcholine (PC) lipid bilayer [1, 21, 30, 31]. Order parameters can be accurately measured in experiments and straightforwardly compared to simulations [32], therefore the molecular electrometer allows the comparison of binding affinity between simulations and experiments.

In this paper, We will show that the response of order parameters to penetrating cations is qualitatively correct in simulations, but the affinity of Na^+ ions for PC bilayers is significantly overestimated in several MD simulation models. Moreover, we will assay the accuracy of lipid–Ca^{2+} interactions in different models and show that current models are not accurate enough for atomistic resolution interpretation of NMR experiments.

II.   RESULTS AND DISCUSSION

A.   Background: Molecular electrometer in experiments

The molecular electrometer concept is based on the experimental observation that binding of any charged objects on a PC bilayer interface induces systematic changes in the choline β and α segment order parameters [1, 21, 30, 31, 33–38]. Thus, these changes can be used to determine binding affinities of the charged objects. Molecular electrometer was originally devised for cations [21, 30], but further experimental quantification with various positively and negatively charged molecules showed that the choline order parameters S_{CH}^{α} and S_{CH}^{β} in general vary linearly with small amount of bound charge per lipid [1, 30, 31, 33–38]. The empirically observed linear relation can be written as [39]

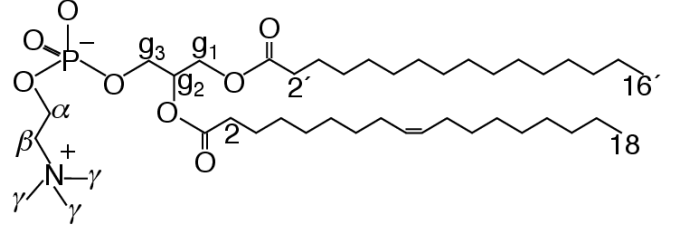$$S_{CH}^i(X^\pm) = S_{CH}^i(0) + \frac{4m_i}{3\chi}X^\pm, \qquad (1)$$

FIG. 1: Chemical structure of 1-palmitoyl-2-oleoylphosphatidylcholine (POPC), and the definition of γ, β, α, g_1, g_2 and g_3 segments.

where $S_{CH}^i(0)$ is the order parameter in the absence of bound charges, m_i empirical constant depending on the valency and position of bound charge, the quadrupole coupling constant $\chi \approx 167$ kHz, $X^\pm$ is the amount of bound charge per lipid, and i refers to either α or β. The order parameter change with respect to a bilayer without bound charges then becomes

$$\Delta S_{CH}^i = S_{CH}^i(X^\pm) - S_{CH}^i(0) = \frac{4m_i}{3\chi}X^\pm. \qquad (2)$$

For Ca^{2+} binding to POPC bilayer (in the presence of 100 mM NaCl), combination of atomic absorption spectra and ^{2}H NMR experiments gave $m_\alpha = -20.5$ and $m_\beta = -10.0$ [30].

The absolute values of order parameters increase for β and decrease for α segment with bound positive charge and *vice versa* for negative charge [1, 21, 30, 31, 33, 38]. However, as the β carbon order parameter is negative while α carbon order parameter is positive [40–42], we can conclude that both ΔS_{CH}^{β} and ΔS_{CH}^{α} decrease with bound positive charge and increase with bound negative charge. Consequently, values of m_i are negative for bound positive charges and *vice versa*. This can be rationalized by electrostatically induced changes in choline P-N dipole tilt [1, 31, 44], which is also seen in simulations [24, 25, 45, 46]. This is in line with order parameter decrease related to the P-N vector tilting more parallel to membrane plane seen with decreasing hydration levels [43].

The quantification of ΔS_{CH}^{β} and ΔS_{CH}^{α} with different cations have revealed that $\Delta S_{CH}^{\beta}/\Delta S_{CH}^{\alpha} \approx 0.5$ for a wide range of different cations (aqueous cations, cationic peptides, cationic anesthetics) [36, 38]. More specifically, the relation $\Delta S_{CH}^{\beta} = 0.43\Delta S_{CH}^{\alpha}$ was found for a DPPC bilayer with various $CaCl_2$ concentrations [21].
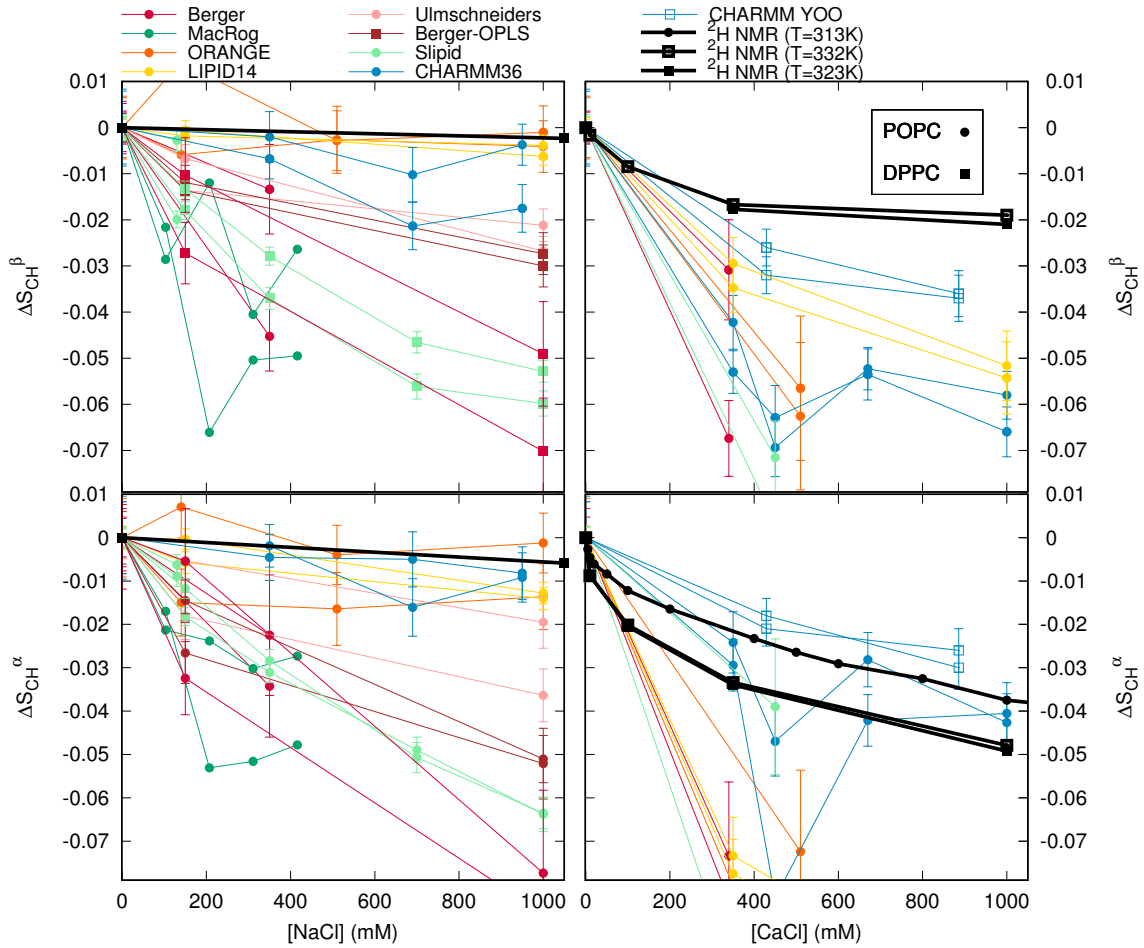
FIG. 2: The order parameter changes for β and α segments as a function of NaCl (left column) and CaCl$_2$ (right column) concentration, from simulations and experiments [21] (POPC with CaCl$_2$ from [30]). The signs of the experimental order parameters, taken from experiments without ions [40–42], can be assumed to be unchanged with concentrations represented here [30, 32]. It should be noted that none of the models used here reproduces the order parameters within experimental error for pure PC bilayer without ions, indicating structural inaccuracies with varying severity in all models [43]. Note that the relatively large decrease in CHARMM36 with 450 mM CaCl$_2$ arise from more equilibrated binding affinity due to long simulation times, see Supplementary Information.

B. Molecular electrometer concept in MD simulations

The headgroup order parameter changes as a function of ion concentration in solution from H^2 NMR experiments are shown in Fig. 2 for DPPC and POPC bilayers [21, 30]. Only minor changes in order parameters are seen as a function of NaCl in solution, while the effect of CaCl$_2$ is an order of magnitude larger. Thus, according to the molecular electrometer concept, monovalent Na$^+$ ions have negligible affinity for PC lipid bilayers at concentrations up to 1 M, while binding of Ca^{2+} ions at the same concentration is significant [21, 30]. (*Note that in contrast to the response as a function of bound charge in Eq. (1), the changes in Fig. 2 are not linear. This can be explained by electrostatic repulsion between already bound calcium ions and ions in solution [30].* **1.Is this really needed? The x-axis of Fig. 2 is not $X^\pm$, so why would one even expect the curves to follow Eq. (1)?**)

Figure 2 also reports order parameter changes calculated

from MD simulations of DPPC and POPC lipid bilayers as a function of NaCl or CaCl$_2$ concentrations in solution (for details of the simulated systems see Table I and Supplementary Information). Note that none of these MD models reproduced within experimental uncertainty the order parameters for a pure PC bilayer without ions (Figure 2 in Ref. [43]), indicating structural inaccuracies of varying severity in all models [43]. However, the experimentally observed headgroup order parameter increase with dehydration was qualitatively reproduced by all the models [43], and similarly here the presence of cations leads to the decrease of S_{CH}^β and S_{CH}^α (Fig. 2), in qualitative agreement with experiments. The changes are, however, overestimated by most models.

Does the molecular electrometer work in MD simulations? According to the molecular electrometer concept, order parameter changes are linearly proportional to the amount of bound cations in bilayer (Eq. (2)). Figure 3 shows the order
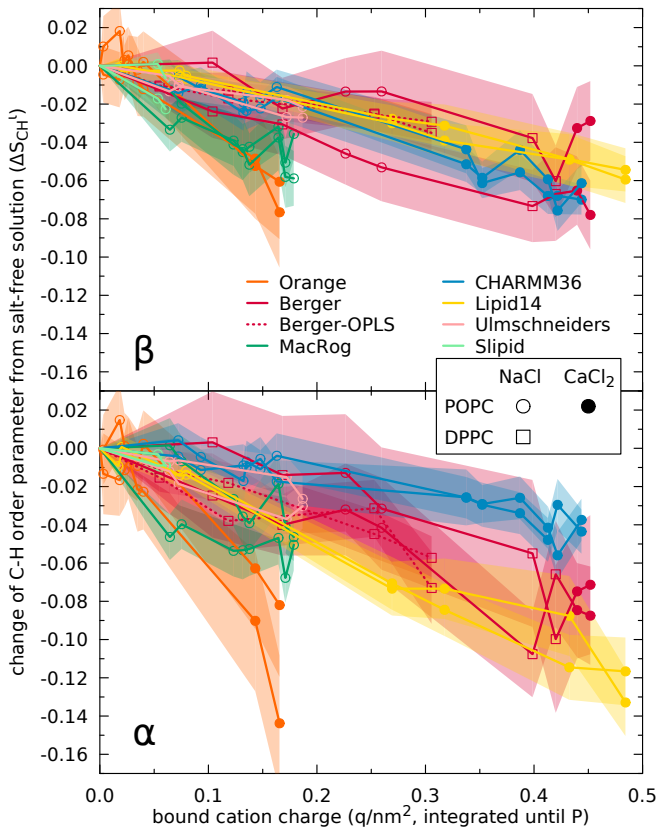
FIG. 3: Order parameters changes $\Delta S^{\beta}_{\mathrm{CH}}$ and $\Delta S^{\alpha}_{\mathrm{CH}}$ as a function of bound cations from different simulation models.

2. Results from long CHARMM and Slipids simulations to be added. Description of the calculation of bound charges to be described, probably in supplementary.

FIG. 4: Relation between $\Delta S^{\beta}_{\mathrm{CH}}$ and $\Delta S^{\alpha}_{\mathrm{CH}}$ from experiments [21] and different simulation models. Solid line is $\Delta S^{\beta}_{\mathrm{CH}} = 0.43 \Delta S^{\alpha}_{\mathrm{CH}}$ determined for DPPC bilayer from ^{2}H NMR experiment with various $CaCl_2$ concentrations [21].

parameter changes as a function of bound charge in MD simulations; in keeping with the molecular electrometer, roughly linear correlation between bound charge and order parameter change is found in all models. Note that quantitative comparison of the proportionality constants (i.e. slopes in Fig. 3) between different models and experimental slopes ($m_{\alpha} = -20.5$ and $m_{\beta} = -10.0$ for Ca^{2+} binding in DPPC bilayer in the presence of 100mM NaCl in Eq. 1 [30]) is not straightforward since the simulation slopes depend on the definition used for bound ions.

The comparison of order parameter changes in response to bound charge is more straightforward for systems with charged amphiphiles fully associated in bilayer, as the amount of bound charge is then explicitly known in both simulations and experiments. Such comparison between previously published simulation data [47] and experiments [31, 48] could not rule out overestimation of order parameter response to bound cations (i.e., slopes m_{β} and m_{α}) in a Berger-based model (Supplementary Information). This might, in principle, explain the overestimated order parameter response of Berger model to $CaCl_2$, but not to NaCl (see discussion in Supplementary Information). Extended comparison with different models is left for further studies.
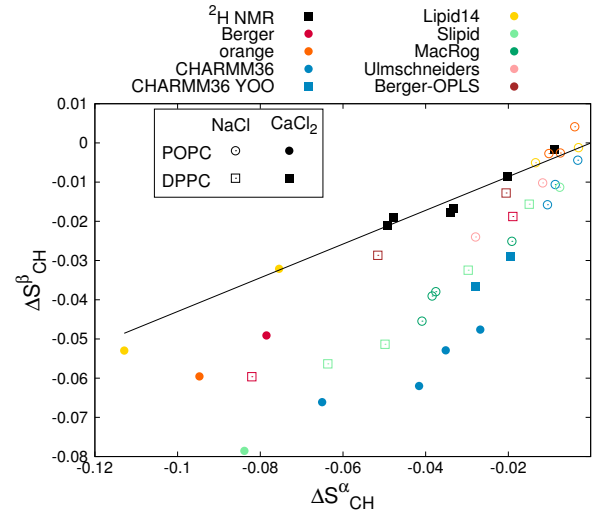
Figure 4 compares the relation between $\Delta S^{\beta}_{\mathrm{CH}}$ and $\Delta S^{\alpha}_{\mathrm{CH}}$

in experiments [21] and different simulation models. Only Lipid14 gives $\Delta S^{\beta}_{\mathrm{CH}}/\Delta S^{\alpha}_{\mathrm{CH}}$ ratio in agreement with the experimental ratio. In all the other models the α order parameter decrease with bound cations is underestimated in respect to β order parameter decrease.

Figure 3 shows that the order parameter decrease clearly correlates with the amount of bound cations also in simulations. This is also evident from Fig. 5, which shows the Na^+ density profiles of the MD models ordered according to the order parameter change (reported in Fig. 2) from the smallest (top) to the largest (bottom). The Na^+ density peaks are larger for models with larger changes in order parameters, in line with the observed correlation between cation binding and order parameter decrease in Fig. 3.

In conclusion, the clear correlation between bound cations and order parameter decrease is observed in all the tested simulation models. Consequently, the electrometer concept can be used to compare the cation binding affinity between experiments and simulations. However, we find that the quantitative response of α and β segment order parameters to bound cations in simulations do not generally agree with the experiments. The $\Delta S^{\beta}_{\mathrm{CH}}/\Delta S^{\alpha}_{\mathrm{CH}}$ ratio agrees with experiments only in Lipid14 model (Fig. 4). Thus, the observed overestimations of the order parameter changes with cation concentrations may, in principle, arise from overbinding of ions or from too sensitive lipid headgroup response on bound cation (see also discussion in Supplementary Information). A careful analysis with current lipid models is performed in the next section.

TABLE I: List of simulations performed in this work. The ion concentrations are calculated as [ion]=($N_{ion}\times$[water])/N_w, where [water]=55.5M. These correspond the concentrations reported in the experiments by Akutsu et al. [21]. The lipid force fields are named as in our previous work [43].

Force field (lipid, ion)	lipid	[Ion] mM	[a]N_l	[b]N_w	[c]N_{Na}	[d]N_{Ca}	[e]N_{Cl}	[f]T (K)	[g]t_{sim}(ns)	[h]t_{anal} (ns)	Files
Berger-POPC-07[49]	POPC	0	128	7290	0	0	0	298	270	240	[50]
Berger-POPC-07[49], ffgmx[51]	POPC	340 (NaCl)	128	7202	44	0	44	298	110	50	[52]
Berger-POPC-07[49], ffgmx[51]	POPC	340 (CaCl$_2$)	128	7157	0	44	88	298	108	58	[53]
Berger-DPPC-97[54]	DPPC	0	72	2880	0	0	0	323	60	50	[55]
Berger-DPPC-97[54], ffgmx[51]	DPPC	150 (NaCl)	72	2880	8	0	8	323	120	60	[56]
Berger-DPPC-97[54], ffgmx[51]	DPPC	1000 (NaCl)	72	2778	51	0	51	323	120	60	[57]
BergerOPLS-DPPC-06[58]	DPPC	0	72	2880	0	0	0	323	120	60	[59]
BergerOPLS-DPPC-06[58], OPLS[60]	DPPC	150 (NaCl)	72	2880	8	0	8	323	120	60	[61]
BergerOPLS-DPPC-06[58], OPLS[60]	DPPC	1000 (NaCl)	72	2778	51	0	51	323	120	60	[62]
CHARMM36[63]	POPC	0	72	2242	0	0	0	303	30	20	[64]
CHARMM36[63], CHARMM36[65]	POPC	350 (NaCl)	72	2085	13	0	13	303	80	60	[66]
CHARMM36[63], CHARMM36[65]	POPC	690 (NaCl)	72	2085	26	0	26	303	73	60	[67]
CHARMM36[63], CHARMM36[65]	POPC	950 (NaCl)	72	2168	37	0	37	303	80	60	[68]
CHARMM36[63], CHARMM36	POPC	350 (CaCl$_2$)	128	6400	0	35	70	303	200	100	[69]
CHARMM36[63], CHARMM36	POPC	450 (CaCl$_2$)	200	9000	0	73	146	310	2000	100	[70]
CHARMM36[63], CHARMM36	POPC	670 (CaCl$_2$)	128	6400	0	67	134	303	200	120	[71]
CHARMM36[63], CHARMM36	POPC	1000 (CaCl$_2$)	128	6400	0	100	200	303	200	100	[72]
CHARMM36[63], Yoo[73]	DPPC	430 (CaCl$_2$)	128	7760	60	0	120	323	200	170	todo
CHARMM36[63], Yoo[73]	DPPC	886 (CaCl$_2$)	128	7520	120	0	240	323	200	170	todo
MacRog[74]	POPC	0	288	14400	0	0	0	310	90	40	[75]
MacRog[74], OPLS[60]	POPC	100 (NaCl)	288	14554	27	0	27	310	90	50	[76]
MacRog[74], OPLS[60]	POPC	210 (NaCl)	288	14500	54	0	54	310	90	50	[76]
MacRog[74], OPLS[60]	POPC	310 (NaCl)	288	14446	81	0	81	310	90	50	[76]
MacRog[74], OPLS[60]	POPC	420 (NaCl)	288	14392	108	0	108	310	90	50	[76]
Orange, OPLS[60]	POPC	0	72	2880	0	0	0	298	60	50	[77]
Orange, OPLS[60]	POPC	140 (NaCl)	72	2866	7	0	7	298	120	60	[78]
Orange, OPLS[60]	POPC	510 (NaCl)	72	2802	26	0	26	298	120	100	[79]
Orange, OPLS[60]	POPC	1000 (NaCl)	72	2780	50	0	50	298	120	80	[80]
Orange, OPLS	POPC	510 (CaCl$_2$)	72	2802	0	26	52	298	120	60	[81]
Slipid[82]	DPPC	0	128	3840	0	0	0	323	150	100	[83]
Slipid[82], AMBER[84, 85]	DPPC	150 (NaCl)	600	18000	49	0	49	323	100	40	-
Slipid[82], AMBER[84, 85]	DPPC	350 (NaCl)	128	3726	57	0	57	323	100	100	[86]
Slipid[82], AMBER[84, 85]	DPPC	700 (NaCl)	128	3612	114	0	114	323	100	100	[86]
Slipid[82], AMBER[84, 85]	DPPC	1000 (NaCl)	128	3514	163	0	163	323	100	100	[86]
Slipid[87]	POPC	0	128	5120	0	0	0	303	200	150	[88]
Slipid[87], AMBER[89]	POPC	130 (NaCl)	200	9000	21	0	21	310	105	100	[90]
Slipid[87], AMBER[60]	POPC	450 (CaCl)	200	9000	0	73	146	310	2000	100	[91]
Lipid14 [92], AMBER[60]	POPC	0	128	5120	0	0	0	298	205	200	[93]
Lipid14 [92], AMBER[60]	POPC	150 (NaCl)	128	5120	12	0	12	298	205	200	[94]
Lipid14 [92], AMBER[60]	POPC	1000 (NaCl)	128	5120	77	0	77	298	205	200	[95]
Lipid14 [92], AMBER[60]	POPC	350 (CaCl$_2$)	128	6400	0	35	70	298	200	100	[96]
Lipid14 [92], AMBER[60]	POPC	1000 (CaCl$_2$)	128	6400	0	100	200	298	200	100	[97]
Ulmschneiders [98], OPLS[60]	POPC	0	128	5120	0	0	0	298.15	205	200	[99]
Ulmschneiders [98], OPLS[60]	POPC	150 (NaCl)	128	5120	12	0	12	298.15	205	200	[100]
Ulmschneiders [98], OPLS[60]	POPC	1000 (NaCl)	128	5120	77	0	77	298.15	205	200	[101]

[a] The number of lipid molecules
[b] The number of water molecules
[c] The number of Na$^+$ molecules
[d] The number of Ca^{2+} molecules
[e] The number of Cl molecules
[f] Simulation temperature
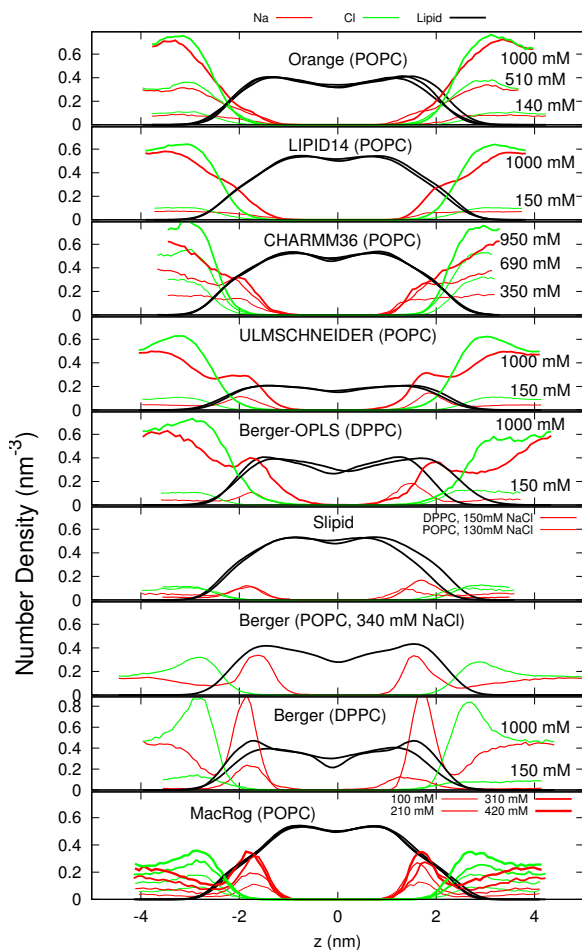[g] The total simulation time

FIG. 5: Atom number density profiles along the membrane normal for lipids, Na$^+$, and Cl$^-$ ions from simulations with different force fields and different NaCl concentrations. The force fields are ordered according to the order parameter changes reported Fig. 2, from the smallest (top panel) to the larges (bottom panel). The lipid densities are scaled by 100 (united atom) or 200 (all atom model) to improve readability. Figure discussed in
https://github.com/NMRLipids/lipid_ionINTERACTION/issues/4.

C. Cation binding in different simulation models

The order parameter changes (Fig. 2) and density distributions (Fig. 5) demonstrate significantly different Na$^+$ binding affinities in different simulation models. The best agreement with experiments (lowest $\Delta S_{\mathrm{CH}}^{\alpha}$ and $\Delta S_{\mathrm{CH}}^{\beta}$) is observed for those models (Orange, CHARMM36, and Lipid14; see Fig. 2) that also predict the lowest Na$^+$ densities in the membrane proximity (Fig. 5). In all the other tested models, the choline order parameter responses to NaCl are clearly overestimated (Fig. 2), and the strength of the overestimation is clearly linked to the strength of the Na$^+$ binding affinity (compare Figs. 2 and 5); this leads us to conclude that sodium binding affinity is overestimated in all these models.

In the best three models, the order parameter changes with

NaCl are small (< 0.02), so with the achieved statistical accuracy we cannot conclude which of the three has the most realistic Na$^+$ binding affinity, especially at physiological NaCl concentrations (~ 150mM) relevant for most applications. The overestimated binding in the other models raise questions on the quality of the predictions from these models when NaCl is present. **3.It has been suggested that we should add references here. The problem is that there are a lot of them and it is difficult to choose which ones to pick. Any opinions?** *Mention that there are many (hundreds?) of them in Web of Science? -markus.* Especially interactions between charged molecules and lipid bilayer might be significantly affected by the strong Na$^+$ binding, as it makes the bilayer effectively positively charged.

Significant Ca^{2+} binding affinity to a phosphatidylcholine bilayer at mM concentrations is agreed in the literature [3, 4, 21, 30], however, several details are yet under discussion. Simulations suggest that Ca^{2+} bind to lipid carbonyl oxygens with coordination number of 4.2 [14], while interpretation of NMR and scattering experiments suggest that one Ca^{2+} interacts mainly with choline groups [102–104] of two phospholipid molecules [30]. Simulation model correctly reproducing the order parameter changes would resolve the discussion by giving atomistic resolution interpretation for the experiments.

As a function of CaCl$_2$ concentration, all but one (CHARMM36 with recent ion model by Yoo et al. [73]), model overestimate the order parameter decrease (Fig. 2). According to the molecular electrometer, this indicates overestimated Ca^{2+} binding. This is the most likely scenario for the models where changes in both order parameters were overestimated, however, in the case of CaCl$_2$ we cannot exclude the possibility that the headgroup response is oversensitive to bound cations (see Supplementary Information). In CHARMM36 with ion model by Yoo et al. [73], ΔS_{CH} is overestimated for β but underestimated for α, in line with Fig. 4 where $\Delta S_{\mathrm{CH}}^{\beta}/\Delta S_{\mathrm{CH}}^{\alpha}$ ratio in CHARMM36 is larger than in experiments. Since we do not know if $\Delta S_{\mathrm{CH}}^{\beta}$ or $\Delta S_{\mathrm{CH}}^{\alpha}$ is more realistic in CHARMM36, we cannot conclude if Ca^{2+} binding is too strong or weak in this simulation model. This could be resolved by comparing CHARMM36 model to the experimental data with known amount of bound charge (e.g., experiments with amphiphilic cations [31, 48]), however, this is beyond the scope of the current work.

The ion density distributions with CaCl$_2$ in Fig. 6 show significant Ca^{2+} binding in all models, however, some differences occur between different models. The Berger model predicts deeper penetration depth (density maxima close to ± 1.8 nm) compared to other models (density maxima close to ± 2 nm). The latter value is probably more realistic since ^{1}H NMR and neutron scattering data indicate that Ca^{2+} interacts mainly with the choline group [3, 102–104]. In CHARMM36, almost all Ca^{2+} ions present in simulation bind in bilayer indicating strongest binding affinity among the tested models. The difference is not as clear in Fig. 2 because α carbon order parameters are least sensitive to bound charge in CHARMM36 (Fig. 3).

The origin of inaccuracies in lipid–ion interactions and binding affinities in different models is far from clear. Potential candidates could be, for example, discrepancies in the
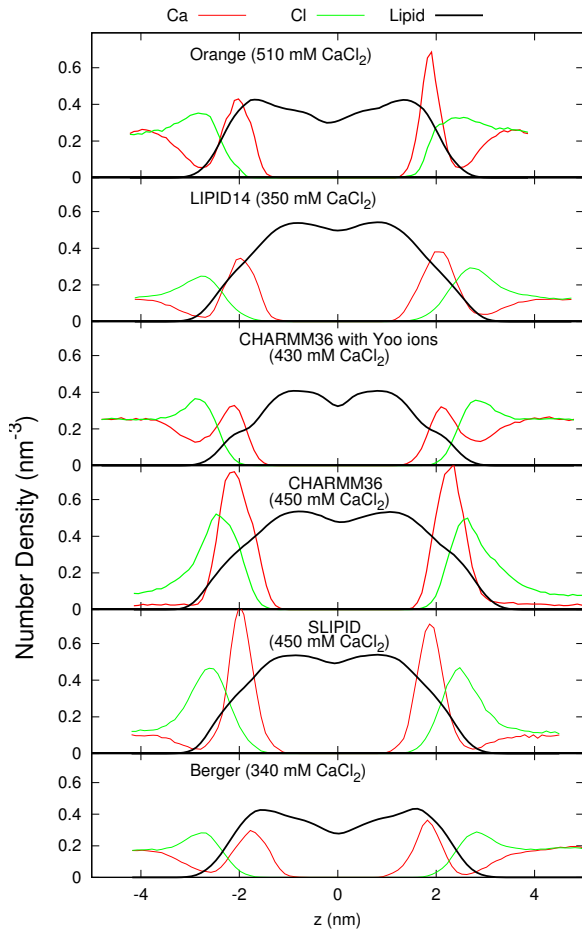
FIG. 6: Atom number density profiles along the membrane normal coordinate z for lipids, Ca^{2+} and Cl^- ions from simulations with different force fields. The profiles only with smallest available $CaCl_2$ concentration are shown for clarity. Figure including all the available concentrations is shown in the Supplementary Information. The lipid densities are scaled with 100 (united atom) or 200 (all atom model) to make them visible with the used y-axis scale. The Cl^- density is scaled with 2 to equalize charge density of ions. Figure discussed in https://github.com/NMRLipids/lipid_ionINTERACTION/issues/4.

Significant reduction of Ca^{2+} binding was observed with ion model by Yoo et al [73], however, the CHARMM36 lipid model must be further analyzed to fully interpret the results.

On the other hand, also the lipid models may have significant influence on ion binding behaviour. For example, the same ion model and non-bonded parameters are used in the Orange and BergerOPLS [58] simulations, but while Na^+ ion binding affinity appears realistic in the Orange model, it is significantly overestimated in the BergerOPLS (Fig. 5). However, realistic Na^+ binding does not directly relate to realistic Ca^{2+} binding (see Orange, Lipid14 and CHARMM36 in Fig. 2) or realistic choline order parameter response to bound charge (see Orange and CHARMM36 in Fig. 4). It should be also noted that the low binding affinity of Na^+ in CHARMM36 model is due to the additional repulsion added between sodium ions and lipid oxygens (NBFIX) [65] (Supplementary Information). Altogether, our results indicate that probably both, lipid and ion force field parameters, need improvement to correctly predict the cation binding affinity, and the associated structural changes.

III. CONCLUSIONS

As suggested by the molecular electrometer concept [1, 21, 30, 31], the decrease in order parameters of α and β carbons in the PC head group of lipids bilayers is related to cation binding in all tested simulation models (Fig. 3), despite of known inaccuracies in the actual atomistic resolution structures [43]. Hence molecular electrometer allows direct comparison of Na^+ binding affinity between simulations and non-invasive NMR experiments. The comparison reveals that most models overestimate Na^+ binding; only Orange, Lipid14, and CHARMM36 predict realistic binding affinity. None of the tested models has the required accuracy to interpret the Ca^{2+}:lipid stoichiometry or induced structural changes with atomistic resolution.

In general, our results support the traditional (pre-2000) view that, in contrast to Ca^{2+} and other multivalent ions [2–5, 11, 12, 20, 21, 29, 30], Na^+ and other monovalent ions (except Li^+) do not specifically bind to the phospholipid bilayer at mM concentrations. Concerning contradictions in the MD simulation results, we reinterpret strong Na^+ binding as an artifact of several simulation models, e.g., the Berger model used in Refs. [13, 14]. Concerning the experimental results, our work sustains the views of Cevc [3], suggesting that the observed small shift in phase transition temperature could be interpreted by other phenomena than Na^+ binding, and the work of Filippov et al. [12] proving that the results of Refs. [8, 10, 13] could be alternatively interpreted by direct interactions between Na^+ ions and fluorescent probes. *Finally, it is questionable if the resolution of AFM experiments [15–19] alone is sufficient to measure ion locations in fluid–like lipid bilayer systems.* **4.This feels like a detached comment…Could we back this claim up, or rephrase? I mean, now it sounds a bit like we came to conclude based on our simulations that the AFM resolution is not enough.**

OLLILA: Rephrasing is welcomed. In the the end, my justification for this comment is that spectrocopy is in general more reliable for atomistic resolution infor-

ion models [105–107], incomplete treatment of electronic polarizability [108], or inaccuracies in the lipid headgroup description [43]. Cordomi et al. [25] showed that the Na^+ binding affinity decreases when ion radius increases in the model, however, also the models with the largest radius show significant binding in DPPC bilayer simulated with OPLS-AA force field [109]. In our results, the Slipid model gives essentially similar binding affinity with ion parameters from Refs. [89] and [84, 85]. Further, the compensation of missing electronic polarizability by scaling ion charge [108, 110] reduced Na^+ binding in Berger, BergerOPLS and Slipid models, but not enough to be in agreement with experiments (Supplementary Information). The charge-scaled Ca^{2+} model [111] slightly reduced binding in CHARMM36, but did not have significant influence on binding in Slipids (Supplementary Information).

The artificial specific Na^+ binding in simulations may lead to doubtful results, since it effectively leads to positively charged phoshatidylcholine (PC) lipid bilayers even at physiological NaCl concentration. Such PC a bilayer has distinctly different interactions with charged objects compared to a (more realistic) model without specific Na^+ binding. Furthermore, the overestimation of Na^+ binding affinity may extend also to other positively charged objects, say, membrane protein segments. This would affect lipid–protein interactions and could explain, for example, contradicting results on electrostatic interactions between charged protein segments and lipid bilayer [112, 113]. In conclusion, more careful studies and model development on lipid bilayer–charged object interactions are called for to make molecular dynamics simulations directly usable in a physiologically relevant electrolytic environment.

This work has been, and will be, progressed and discussed through the blog `nmrlipids.blogspot.fi`, through which everyone is invited to join the discussion and make contributions. The manuscript will be eventually submitted to an appropriate scientific journal. Everyone who has contributed to the work through the blog will be offered coauthorship. For more details see `nmrlipids.blogspot.fi`.
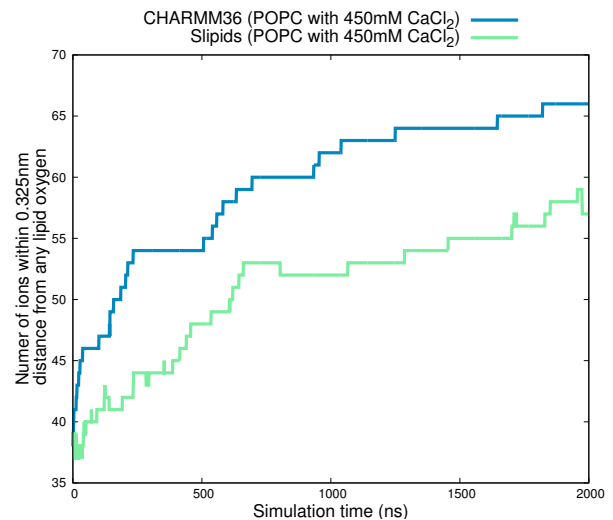
FIG. 7: Number of bound Ca^{2+} as a function of time from 2 μs long simulations with CHARMM36 and Slipids.

SUPPLEMENTARY INFORMATION

Appendix A: Ion binding equilibration times

Simulations containg 450 mM $CaCl_2$ with CHARMM36 and Slipids were ran 2 μs to estimate the times required to equilibrate amount of bound Ca^{2+} in lipid bilayer. The amount of the bound calcium as a function of simulation time from these simulations are shown in Fig. 7. The results show clear increase in binding affinity up to 1000 ns and 700 ns in CHARMM36 and Slipids, respectively, and moderate increase even after this. This is also reflected to the CHARMM36 results in Fig. 2, where long CHARMM36 simulation with 450 mM $CaCl_2$ show relatively lower order parameters than shorter simulations. This can be rationalized with higher and more equilibrated binding affinity in long simulations. The results suggest that in other simulations the binding affinity is underestimated due to the insufficient equilibration times. This should be taken into account in more careful studies, but do not interfere the conclusion in this work that Ca^{2+} binding is most likely overestimated in all the other models than CHARMM36 with ion model by Yoo et al. [73].

Appendix B: Headgroup response on charged amphiphiles

The order parameter changes as a function of the bound charge cannot be straightforwardly compared between simulations and experiments from systems with ions because the results depend on the definition of bound ions in simulations. In systems with charged amphihiles the situation is more straightforward since all the charges can be assumed to locate in bilayer in both, simulations and experiments. The order parameter changes as a function of charged amphiphiles, cal-

FIG. 8: Order parameter changes as a function of cationic amphihiles from simulations [47, 114–116] and experiments [31, 48]. Experimental points for binary mixtures of POPC and 1,2-dioleoyloxy-3-(trimethylammonio)propane (DOTAP) are from [48]. Experimental lines are from $\Delta S_{\mathrm{CH}}^{i} = \frac{4}{3}\chi^{-1}m_i X^{\pm}$, where m_i are taken as average for different amphiphiles measured in [31].

culated from previously published simulation data [47, 114–116] and experiments [31, 48], is shown in Fig 8.

The simulation data is from previously published binary mixture of cationic dimyristoyltrimethylammoniumpropane (DMTAP) and zwitterionic (neutral) dimyristoylphosphatidyl-choline (DMPC) [47, 114–116], simulated with Berger based model. This is compared to experimental data from binary mixtures of POPC and various cationic amphiphiles [31, 48].

The order parameter changes from simulations overestimate the changes measured from DMPC/DOTAP mixtures [48] especially with larger amphiphile concentrations, but are in good agreement with experimental line from various amphiphiles with saturated acyl chains measured by Scherer et al. [31]. The origin of the difference in order parameter changes between DOTAP and amphihiles with saturated chains is not known. It may arise from the differecens in acyl chain saturation level or from differences in headgroup. In the used simulation data the acyl chains are similar to data from [31] but the headgroup is similar to the data from [48]. Also Cl^{-} binding affinity may affect the comparison. Thus

we cannot fully conclude how well the headgroup response to bound charge is reproduced in simulation.

To estimate the maximum error we take the maximum amount of bound charge from Fig. 3 ($\approx 0.5\frac{\mathrm{e}}{\mathrm{nm}^2}$) and assume the area per lipid of 0.68 nm². This gives for maximum amount of bound charge per lipid $X_{\max}^{+} = 0.5\frac{\mathrm{e}}{\mathrm{nm}^2} \cdot 0.68\frac{\mathrm{nm}^2}{\mathrm{lipid}} = 0.34\frac{\mathrm{e}}{\mathrm{lipid}}$, which is shown as dashed line in Fig. 8. The maximum overestimations of order parameter decrease with this amount of bound charge per lipid are ≈ 0.04 and ≈ 0.06 for β and α order parameter changes, respectively. The numbers are smaller with less amount of bound cations. In principle, these values could explain the overestimated order parameter change due to the presence of $CaCl_2$ in Berger model but not in the presence of NaCl (see Fig. 2).

In conclusion, we cannot fully exclude the possibility that the overestimated order parameter response to the $CaCl_2$ with Berger model arises from oversensitive headgroup response to bound cations with the current data. However, in the presence of NaCl the differences between responses in simulations and experiments in Fig. 2 are larger than the maximum estimated influence from a possible oversensitivity of the headgroup.

Appendix C: Density distributions with different $CaCl_2$ concentrations

The density distributions with all simulated $CaCl_2$ concentrations are shown in Fig. 9.

Appendix D: Effect of ion model and polarization

It has been suggested that the missing electronic polarizability can be compensated by scaling the ion charge in simulations [108]. To test if this would improve the Na^{+} ion binding behaviour, we ran simulations with Berger-DPPC-97, BergerOPLS-DPPC-06 and Slipids with scaled Na^{+} and Cl^{-} ions. For Berger-DPPC-97 and BergerOPLS-DPPC-06 models the ion charge in systems listed in Table I was simply scaled with 0.7 and the related files are available at [117–120]). For simulations with Slipids the ion model by Kohagen et al. was used [110] and the related files are available at [121]. The simulation parameters were identical to those employed in the simulation of POPC with 130 mM NaCl (see Methods). The order parameter changes and Na^{+}-binding affinity are decreased by the charge scaling but yet overestimated with respect to the experiments as seen from Figs. 10 and 11. Thus the overestimated binding affinity cannot be fixed by only scaling the charges of ions.

The ion model for $CaCl_2$ with scaled charges [111] was tested with CHARMM36 and Slipid models. The related files are available at [122] and [123], respectively, and the results are shown in Figs. 10 and 9. The results with scaled charges are slightly improved but yet far from experiments.

Figure 10 also compares CHARMM36 simulation [124] with and without NBFIX [65] for NaCl. As expected, without NBFIX the order parameter decrease is more significant. **5.Discussion will be finished as soon as we have the density profiles. Citations to Zenodo**

FIG. 9: Number density profiles for lipids, Ca^{2+} and Cl^- ions from simulations with different force fields and different $CaCl_2$ concentrations. The lipid densities are scaled with 100 (united atom) or 200 (all atom model) to make them visible with the used y-axis scale. The Cl^- density is scaled with 2 to equalize charge density of ions. Figure discussed in https://github.com/NMRLipids/lipid_ionINTERACTION/issues/4.

repositories will be added, if available. JM: added, please, check. Because the difference promoted by NBFIX [65] is mainly a reduced Na^+ density in the headgroup region of the phospholipids, this behaviour suggests that it is the direct interaction between the lipids and the Na^+ cation (and to no or much lesser extent Cl^- anions) that drives the changes of the order parameters.

Appendix E: methods

1. Simulated systems

All simulations are ran with a standard setup for planar lipid bilayer in zero tension with periodic boundary conditions with Gromacs (version numbers 4.5-X-5.0.X) [125, 126] or NAMD [127] software packages.

2. Analysis

The order parameters were calculated from simulation trajectories directly applying the equation $S_{CH} = \langle \frac{3}{2} \cos^2 \theta - \frac{1}{2} \rangle$, where θ is the angle between a given C–H bond and the bilayer normal, and the average is taken over all lipids and time frames. For united atom models, the positions of hydrogen atoms were calculated for each molecule in each frame *a posteriori* by using the *g_protonate* tool in Gromacs 4.0.2 [128]. The statistical error in the order parameter was estimated by calculating the average value separately for each lipid molecule, and then the average and standard error of the mean over the ensemble of lipids (as done also in previous work [43]). All the scripts used for analysis and the resulting data are available in the GitHub repository [129]

3. Simulation details

a. Berger

POPC: The simulation without ions is the same as in [130] and the files are available at [50]. The starting structures for simulations with ions is made by replacing water molecules with appropriate amount of ions (see Table I). The Berger force field was used for the POPC [131], with the dihedral potential next to the double bond taken from [132]. The ion parameters from ffmgx [51] were used. Timestep of 2 fs was used with leap-frog integrator. Covalent bond lengths were constrained with LINCS algorithm [133, 134]. Coordinates were written every 10 ps. PME [135, 136] with real space cut-off at 1.0 nm was used for electrostatics. Plain cut-off was used for the Lennard-Jones interactions with a 1.0 nm cut-off. The neighbour list was updated every 5th step with cut-off at 1.0 nm. Temperature was coupled separately for lipids, water and ions to 298 K with the velocity-rescale method [137] with coupling constant 0.1 ps^{-1}. Pressure was semi-isotropically coupled to the athmospheric pressure with the Parrinello–Rahman barostat [138].

DPPC: The simulation without ions is the same as in [43] and the files are available at [55]. The initial configuration contained 72 DPPC lipids and 2880 SPC water molecules. The standard Berger DPPC force field was used [131] (simulations indicated as Berger-DPPC-97 in Table I). The electrostatics were handled with PME [135, 136], with real-space Coulomb cut-off set at 1.0 nm. Lennard-Jones potentials were cut off at 1.0 nm. The neighbor list for all non-bonded interactions was updated every 10 steps. Temperature was set to 323K with the velocity-rescale method [137] using a coupling constant of 0.1 ps^{-1}. Semi-isotropic pressure coupling at 1 atm was handled with the Parrinello-Rahman barostat [138] with 1 ps coupling constant. The time step was 4 fs, and coordinates were written every 10 ps. The total simulation time was 120 ns (without pre-equilibration) and last 60 ns was used in the order parameter analysis.

For simulations with added salt, the appropriate number of SPC water molecules were randomly replaced with ions. Ions were described by the ffgmx parameters [51]. In simulations
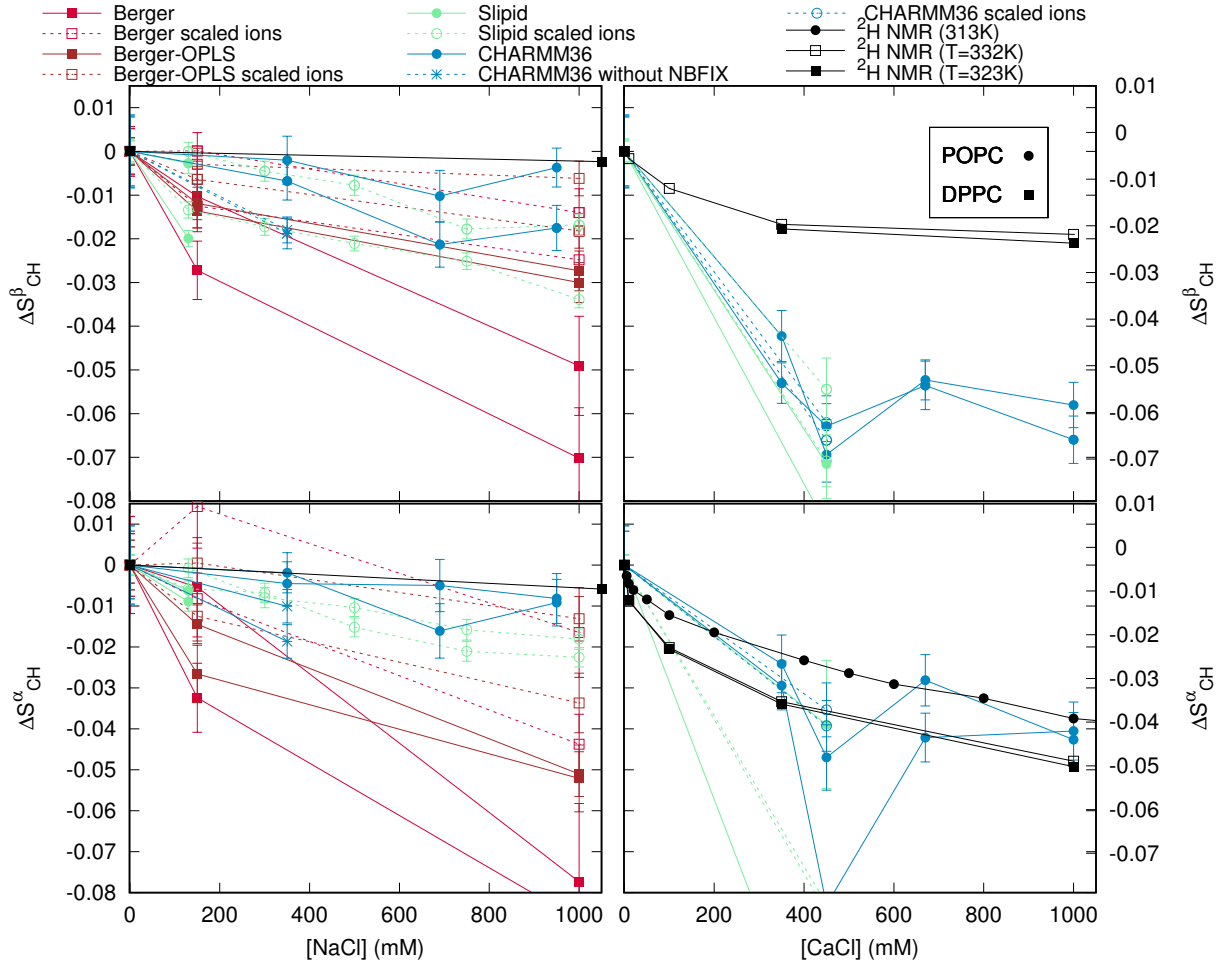
FIG. 10: The effect of charge scaling [108, 111] and NBFIX [65] on order parameter changes in simulations.

with scaled charges, charge-scaling was applied by scaling the ion charges by a factor 0.7. Conditions in the ion simulations were as with the pure DPPC described above. The duration of the simulations was 120 ns (without pre-equilibration) and last 60 ns was used in the order parameter analysis.

All the simulation files for pure DPPC simulations can be found at [55] and for the simulations with ions at [56, 57] and with scaled ions at [117, 118].

b. BergerOPLS

For simulations without ions, the initial configuration contains 72 DPPC lipids and 2880 SPC water molecules. For simulations with added salt, the appropriate amount of SPC water molecules were randomly replaced with ions. The number of ions is reported in Table I. For the lipids, we used the same version of Berger force field as in previous simulations, described in [131]; for the ions, we used the Åqvist parameters [60] (commonly used within the OPLS-AA force field). Issues related to the compatibility between Berger and OPLS-AA force fields are described in ref. [58]. A set of simulations was carried out using reduced electrostatic charges on the ions; in

this case, a charge of 0.7 e was used on the ions, as described in refs. [108, 110]. Except for the ion force field, all simulation parameters (for non-bonded interactions, integration time step, thermostat, etc.) were identical to the parameters used in the Berger DPPC simulations described above.

All simulation files can be found at [59] for pure DPPC simulations, at [61, 62] for simulations with ions, and at [119, 120] for simulations with ions with scaled charges.

c. CHARMM36

POPC with NaCl: The simulation without ions is taken directly from [43, 64]. The starting structures for simulations with NaCl were made by replacing randomly located water molecules of the structure of pure POPC simulation with appropriate amount of ions. The force field for lipid were the same as in [43, 64]. The ion parameters with NBFIX by Venable et al. [65] were used. Simulations were ran with Gromacs 4.5.5 software [125]. Timestep of 2 fs was used with leap-frog integrator. Covalent bonds with hydrogens were constrained with LINCS algorithm [133, 134]. Coordinates were written every 5 ps. PME with real space cut-off 1.4 nm was used

FIG. 11: Atom number density profiles along membrane normal coordinate z for lipids, Na^+ and Cl^- ions from simulations using ion models with scaled charges. The lipid densities are scaled with 100 (united atom) or 200 (all atom model) to make them visible with the used y-axis scale.

for electrostatics. Lennard-Jones interactions were switched to zero between 0.8 nm and 1.2 nm. The neighbour list was updated every 5th step with cut-off 1.4 nm. Temperature was coupled separately for lipids and solution to 303 K with the velocity-rescale method [137] with coupling constant 0.2 ps. Pressure was semi-isotropically coupled to the athmospheric pressure with the Berendsen method [139].

Also simulation without NBFIX [65] was run to check its effect on Na^+ binding. **6.J. Melcr: DONE** The simulation settings were kept consistent with the simulations with NBFIX. The temperature was kept at 310 K with Nosé–Hoover [140, 141] thermostat. The simulation files are available at [124].

POPC with CaCl$_2$: The starting structures with varying amounts of $CaCl_2$ were constructed using the CHARMM-GUI Membrane Builder (http://www.charmm-gui.org/) online tool [142]. All runs were performed with Gromacs 5.0.3 software package [126] and CHARMM36 additive force field parameters for lipids [63] and ions were obtained from CHARMM-GUI input files. Simulation parameters provided by CHARMM-GUI were used. Particularly, the lenghts of the bonds involving hydrogens were constrained with LINCS [133, 134]. The temperatures of the lipids and the solvent were separately coupled to the Nose–Hoover [140, 141] thermostat with a target temperature of 303 K and a relaxation time constant of 1.0 ps. Semi-isotropical pressure coupling to 1 bar was obtained with the Parrinello-Rahman barostat [138] with a time constant of 5 ps. Equations of motion were integrated with the Verlet algorithm [143] using a timestep of 2 fs. Long-range electrostatic interactions were calculated using the PME [135, 136] method with a fourth order smoothing spline. A real space cut-off of 1.2 nm was employed with grid spacing of 0.12 nm in the reciprocal space. Lennard-Jones interactions were smoothly switched to zero between 1.0 nm and 1.2 nm. Verlet cutoff-scheme [143] was used with the long-range neighbor list updated every 20 steps. Coordinates were written every 10 ps. After energy minimization and an

equilibration run of 0.5 ns, 200 ns simulations were ran and the last 100 ns of each simulation was employed for the analysis.

DPPC with CaCl$_2$ (Yoo model): The systems contained 128 DPPC lipids and about 7600 TIP3P water molecules, and an appropriate amount of ions as indicated in Table I. We have used CHARMM36 additive force field parameters for lipids [63]. In the calcium model developed recently by Yoo et al. [73], each cation is decorated by seven hydrating water molecules (with different charges from the usual TIP3P), which are constrainted to remain in its vincinity. The associated parameter files are available on http://bionano.physics.illinois.edu/CUFIX. The constraint on the calcium-oxygen distances was imposed by adding extra-bonds through a harmonic potential $V(r) = k(r - r_0)^2$, with $r_0 = 2.25$ Å and $k = 10$ kcal·mol^{-1}·Å^{-2}.

The starting configuration of hydrated lipidic bilayers were constructed using *packmol* [144] with a large area per lipid (74 Å^2). After a first energy minimization (5000 steps), varying amounts of Ca^{2+} and Cl^- ions were added by replacing water molecules, using the *autoionize* plugin of vmd package [145], mentionning explicitly the number of ions required. Ion placement is random, with the constraint of minimum 5 Å between ions and lipids, as well as between any two ions. A second energy minimization was performed after inserting the ions.

All the minimizations and dynamics were conducted using the NAMD package [127]. The temperature of the whole system was controled with Langevin thermostat with a target temperature of 323 K and a relaxation time constant of 1 ps. The modified NAMD version of Nose–Hoover barostat with Langevin dynamics (piston period of 0.1 ps and piston decay time of 0.05 ps) was used semi-isotropically for an average target pressure of 1 bar and an average zero surface tension. The equations of motion were integrated using the multiple time step Verlet r-RESPA algorithm [143] with a time step of 2 fs, and electrostatic forces calculated only every two time steps. Covalent bonds between heavy and hydrogen atoms were constrained using SHAKE/RATTLE algorithm. Long-range electrostatic interactions were calculated using the PME [135, 136] method with a 4-th order smoothing spline and a grid spacing of about 0.1 nm. A cut-off of 1.2 nm was employed for the Lennard-Jones interactions, with a force-based switching function for distances beyond 1 nm. Neighbor lists with a radius of 1.4 nm were updated every 10 timesteps. Coordinates were written every 20 ps. After energy minimization, a run of 200 ns simulations was performed, and the last ∼ 170 ns of trajectory was employed for the analysis. Error bars are defined by ± the standard error of the mean, taking into account the correlation time of the average order parameters (200 ps for 430 mM and 400 ps for 890 mM).

d. MacRog

The simulation parameters are identical to those employed in our earlier study [43] for the full hydration and dehydration simulations. The initial structures with varying amounts of

NaCl were constructed from an extensively hydrated bilayer by replacing water molecules with ions using the Gromacs *genion* tool [146]. Even at the highest considered salt concentration, the amount of water molecules per lipid after this replacement process was still greater than 50.

e. Orange

The systems contained 72 POPC lipids and 2880 SPC water molecules, and an appropriate amount of ions as indicated in Table I.

For the lipids, we used an unpublished force field coined Orange force field. Briefly, this includes most bonded interactions from Berger lipids [131], except for dihedrals which were derived via *ab initio* calculations on small model compounds. As in Berger lipids, Lennard-Jones parameters are from OPLS [147–151]. Partial charges were derived on the basis of *ab initio* calculations. In simulations with ions, the Åqvist parameters were used [60]. The electrostatics were handled with PME [135, 136], with real-space Coulomb cut-off set at 1.8 nm. Lennard-Jones potentials were cut off at 1.8 nm. The neighbor lists for the calculation of non-bonded forces were updated every 5 steps.

Temperature was set to 298K with the velocity-rescale thermostat [137] using a coupling constant of 0.1 ps^{-1}, and the pressure was set to 1 bar using the Berendsen weak coupling algorithm [139] (compressibility of $4.5 \cdot 10^{-5}$ bar^{-1}, time constant of 1 ps), coupling separately the x-y dimension and the z dimension to obtain a tensionless system. A time step of 2 fs was used for the integration (with the leap-frog algorithm), coordinates were written every 100 ps, and the total simulation time was 60 ns.

Simulation files for pure lipid simulations are found at [77] and for the simulations with ions at [78–81].

f. Slipids

DPPC: The simulation without ions from [43], available at [83] was used. For the simulation with 150 mM NaCl, the starting DPPC lipid bilayer, which was built with the online CHARMM-GUI [142] (http://www.charmm-gui.org/), contained 600 lipids hydrated by 30 water molecules per lipid. For the simulation at higher NaCl concentrations (350, 700 and 1000 mM), the configuration from [83] was taken and an appropriate amount of water molecules was converted to ions to form a neutral NaCl solution. The simulation files are available at [86]. We used TIP3P water model and ion parameters by Roux [84, 85]. Stockholm lipids (Slipids) force field [82, 87] parameters were used for phospholipids. GROMACS software package version 4.5.5 or 5.0.7 [125] was employed for all simulations. After energy minimization and a short equilibration run of 50 ps (time step 1 fs), 100 ns production runs were performed using a time step of 2 fs with leap-frog integrator. All covalent bonds were constrained with the LINCS [133, 134] algorithm. Coordinates were written every 100 ps. PME [135, 136] with real space cut-off at 1.0

nm was used for Coulomb interactions. Lennard-Jones interactions were switched to zero between 1.0 nm and 1.4 nm. The neighbour lists were updated every 10$^{\text{th}}$ step with a cut-off of 1.6 nm. Temperature was coupled separately for upper and bottom leaflets of the lipid bilayer, and for water to 323 K with the Nosé-Hoover thermostat [140, 141] using a time constant of 0.5 ps. Pressure was semi-isotropically coupled to the atmospheric pressure with the Parrinello-Rahman [138] barostat using a time constant of 10 ps. **7.J. Melcr: done, see above**

POPC: The simulation without ions from [43], available at [88] was used.

POPC with NaCl: A POPC bilayer consisting of 200 lipids, hydrated with 45 water molecules per lipid, was simulated in the presence of 130 mM NaCl. The Slipids model [82, 87] was employed for lipids, the tip3p model [152] for water, and the ion parameters by Smith and Dang [89] for NaCl. The system was first equilibrated for 5 ns with a time step of 1 fs after which a 100 ns production run was performed using a time step of 2 fs. Trajectories were written every 100 ps. The system was kept in a tensionless state at 1 bar using a semi-isotropic Parrinello–Rahman barostat [138] with a time constant of 1 ps. The temperature was maintained at 310 K with the velocity rescaling thermostat [137]. The time constant was set to 0.5 ps for both lipids and solvent (water and ions) which were coupled separately. Non-bonded interactions were calculated within a neighbor list with a radius of 1 nm and an update interval of 10 steps. The Lennard-Jones interactions were cut-off at 1 nm, whereas PME [135, 136] was employed for long-range electrostatics. Dispersion correction was applied to both energy and pressure. All bonds were constrained with the LINCS [133, 134]. algorithm.

POPC with CaCl$_2$: A POPC bilayer consisting of 200 lipids, hydrated with 45 water molecules per lipid, was simulated in the presence of 450 mM CaCl$_2$. The system was ran for 2000 ns and the last 100 ns was used for analysis. Other details are as in POPC with NaCl.

g. Lipid14

The starting structures with varying amounts of ions were constructed using the CHARMM-GUI Membrane Builder (http://www.charmm-gui.org/) online tool [142]. The GROMACS compatible force field parameters generated in [43] and available at [153] were used. The TIP3P water model [152] was used to solvate the system and Åqvist [60] parameters were used for ions. All runs were performed with Gromacs 5.0.3 software package [126] and LIPID14 force field parameters for POPC [92].

H-bond lengths were constrained with LINCS [133, 134]. The temperatures of the lipids and the solvent were separately coupled to the Nose–Hoover [140, 141] thermostat with a target temperature of 298.15 K and a relaxation time constant of 0.1 ps. Semi-isotropic pressure coupling to 1 bar was obtained with the Parrinello-Rahman barostat [138] with a time constant of 2 ps. Equations of motion were integrated with the Verlet algorithm [143] using a timestep of 2 fs. Long-range electrostatic interactions were calculated us-

ing the PME [135, 136] method with a fourth order smoothing spline. A real space cut-off at 1.0 nm was employed with grid spacing of 0.12 nm in the reciprocal space. Lennard-Jones potentials were cut-off at 1 nm, with a dispersion correction applied to both energy and pressure. Verlet cutoff-scheme [143] were used with the long-range neighbor list updated every 20 steps. Coordinates were written every 10 ps.

After energy minimization and an equilibration run of 5 ns, 200 ns production runs were performed and analysed. In case of the $CaCl_2$ systems only the last 100 ns of each simulation was employed for the analysis.

h.   Ulmschneiders

The starting structures with varying amounts of ions were constructed using the CHARMM-GUI Membrane Builder (http://www.charmm-gui.org) online tool [142]. The force field parameters were obtained from Lipidbook [154]. The TIP3P water model [152] was used to solvate the system. Additionally, the simulations of ion-free bilayer were repeated with both Verlet and Group cutoff-schemes [99]. There was no significant difference in headgroup or glycerol backbone order parameters between these cutoff-schemes. All runs were performed with Gromacs 5.0.3 software package [126]. The glycerol backbone order parameters without iones were not the same as reported in the previous study [43]. The origin of discrepancy was located to the different initial structures which was taken from CHARMM-GUI in this work and from Lipidbook in the previous work. Since the order parameters with the initial structure from CHARMM-GUI are closer to the experimental values, the results indicate that the structure available from Lipidbook is stuck to a state with incorrect glycerol backbone strucuture, for more discussion see https://github.com/NMRLipids/lipid_ionINTERACTION/issues/8.

All-bond lengths were constrained with LINCS [133, 134]. The temperatures of the lipids and the solvent were separately coupled to the Nose–Hoover [140, 141] thermostat with a target temperature of 298.15 K and a relaxation time constant of 0.1 ps. Semi-isotropic pressure coupling to 1 bar was obtained with the Parrinello-Rahman barostat [138] with a time constant of 2 ps. Equations of motion were integrated with the Verlet algorithm [143] using a timestep of 2 fs. Long-range electrostatic interactions were calculated using the PME [135, 136] method with a fourth order smoothing spline. A real space cut-off at 1.0 nm was employed with grid spacing of 0.12 nm in the reciprocal space. Lennard-Jones potentials were cut-off at 1 nm, with a dispersion correction applied to both energy and pressure. Verlet cutoff-scheme [143] were used with the long-range neighbor list updated every 20 steps. Coordinates were written every 10 ps. After energy minimization and an equilibration run of 5 ns, 200 ns simulations were ran and the last 100 ns of each simulation was employed for the analysis.

Appendix F: Author Contributions

Andrea Catte
Mykhailo Girych ran and analyzed several simulations. Discussed the project actively with OHSO.
Matti Javanainen provided data with several lipid and ion models. Discussed the project actively with OHSO. Supervised the work of JT.
Claire Loison provided results for CHARMM36 DPPC+$CaCl_2$ with Yoo's model.
Josef Melcr performed and analyzed several simulations; discussed the project actively; corrected and contributed to the manuscript.
Markus S. Miettinen
Luca Monticelli
Jukka Määttä
Vasily S. Oganesyan
O. H. Samuli Ollila co-designed the project with MSM and managed the work. Ran and analyzed several simulations. Wrote the manuscript.
Joona Tynkkynen
Sergey Vilov provided results for CHARMM36 DPPC+$CaCl_2$ with Yoo's model.

TODO

[1] J. Seelig, P. M. MacDonald, and P. G. Scherer, Biochemistry **26**, 7535 (1987).

[2] M. Eisenberg, T. Gresalfi, T. Riccio, and S. McLaughlin, Biochemistry **18**, 5213 (1979).

[3] G. Cevc, Biochim. Biophys. Acta - Rev. Biomemb. **1031**, 311 (1990).

[4] J.-F. Tocanne and J. Teissi, Biochimica et Biophysica Acta (BBA) - Reviews on Biomembranes **1031**, 111 (1990).

[5] H. Binder and O. Zschörnig, Chem. Phys. Lipids **115**, 39 (2002).

[6] J. J. Garcia-Celma, L. Hatahet, W. Kunz, and K. Fendler, Langmuir **23**, 10074 (2007).

[7] E. Leontidis and A. Aroti, The Journal of Physical Chemistry B **113**, 1460 (2009).

[8] R. Vacha, S. W. I. Siu, M. Petrov, R. A. Böckmann, J. Barucha-Kraszewska, P. Jurkiewicz, M. Hof, M. L. Berkowitz, and P. Jungwirth, J. Phys. Chem. A **113**, 7235 (2009).

[9] B. Klasczyk, V. Knecht, R. Lipowsky, and R. Dimova, Langmuir **26**, 18951 (2010).

[10] F. F. Harb and B. Tinland, Langmuir **29**, 5540 (2013).

[11] G. Pabst, A. Hodzic, J. Strancar, S. Danner, M. Rappolt, and P. Laggner, Biophys. J. **93**, 2688 (2007).

[12] A. Filippov, G. Ordd, and G. Lindblom, Chemistry and Physics of Lipids **159**, 81 (2009).

[13] R. A. Böckmann, A. Hac, T. Heimburg, and H. Grubmüller, Biophys. J. **85**, 1647 (2003).

[14] R. A. Böckmann and H. Grubmüller, Ang. Chem. Int. Ed. **43**, 1021 (2004).

[15] S. Garcia-Manyes, G. Oncins, and F. Sanz, Biophys. J. **89**, 1812 (2005).

[16] S. Garcia-Manyes, G. Oncins, and F. Sanz, Electrochimica Acta **51**, 5029 (2006), ISSN 0013-4686, bioelectrochemistry 2005 Bioelectrochemistry 2005, URL http://www.sciencedirect.com/science/article/pii/S0013468606002775.

[17] T. Fukuma, M. J. Higgins, and S. P. Jarvis, Phys. Rev. Lett. **98**, 106101 (2007).

[18] U. Ferber, G. Kaggwa, and S. Jarvis, European Biophysics Journal **40**, 329 (2011), ISSN 0175-7571, URL http://dx.doi.org/10.1007/s00249-010-0650-7.

[19] L. Redondo-Morata, G. Oncins, and F. Sanz, Biophysical Journal **102**, 66 (2012).

[20] R. J. Clarke and C. Lpfert, Biophysical Journal **76**, 2614 (1999).

[21] H. Akutsu and J. Seelig, Biochemistry **20**, 7366 (1981).

[22] J. N. Sachs, H. Nanda, H. I. Petrache, and T. B. Woolf, Biophys. J. **86**, 3772 (2004).

[23] M. L. Berkowitz, D. L. Bostick, and S. Pandit, Chem. Rev. **106**, 1527 (2006).

[24] A. Cordom, O. Edholm, and J. J. Perez, The Journal of Physical Chemistry B **112**, 1397 (2008).

[25] A. Cordomi, O. Edholm, and J. J. Perez, J. Chem. Theo. Comput. **5**, 2125 (2009).

[26] C. Valley, J. Perlmutter, A. Braun, and J. Sachs, J. Membr. Biol. **244**, 35 (2011).

[27] M. L. Berkowitz and R. Vacha, Acc. Chem. Res. **45**, 74 (2012).

[28] V. Knecht and B. Klasczyk, Biophys. J. **104**, 818 (2013).

[29] S. A. TATULIAN, European Journal of Biochemistry **170**, 413 (1987), ISSN 1432-1033, URL http://dx.doi.org/10.1111/j.1432-1033.1987.tb13715.x.

[30] C. Altenbach and J. Seelig, Biochemistry **23**, 3913 (1984).

[31] P. G. Scherer and J. Seelig, Biochemistry **28**, 7720 (1989).

[32] O. S. Ollila and G. Pabst, *Atomistic resolution structure and dynamics of lipid bilayers in simulations and experiments* (2016), in Press, URL http://dx.doi.org/10.1016/j.bbamem.2016.01.019.

[33] C. Altenbach and J. Seelig, Biochim. Biophys. Acta **818**, 410 (1985).

[34] P. M. Macdonald and J. Seelig, Biochemistry **26**, 1231 (1987).

[35] M. Roux and M. Bloom, Biochemistry **29**, 7077 (1990).

[36] G. Beschiaschvili and J. Seelig, Biochimica et Biophysica Acta (BBA) - Biomembranes **1061**, 78 (1991).

[37] F. M. Marassi and P. M. Macdonald, Biochemistry **31**, 10031 (1992).

[38] J. R. Rydall and P. M. Macdonald, Biochemistry **31**, 1092 (1992).

[39] T. M. Ferreira, R. Sood, R. Barenwald, G. Carlstrm, D. Topgaard, K. Saalwaechter, P. K. Kinnunen, and S. O. Ollila, Langmuir **0**, null (0), pMID: 27260273, http://dx.doi.org/10.1021/acs.langmuir.6b00788, URL http://dx.doi.org/10.1021/acs.langmuir.6b00788.

[40] M. Hong, K. Schmidt-Rohr, and A. Pines, Journal of the American Chemical Society **117**, 3310 (1995).

[41] M. Hong, K. Schmidt-Rohr, and D. Nanz, Biophysical Journal **69**, 1939 (1995).

[42] J. D. Gross, D. E. Warschawski, and R. G. Griffin, Journal of the American Chemical Society **119**, 796 (1997).

[43] A. Botan, F. Favela-Rosales, P. F. J. Fuchs, M. Javanainen, M. Kandu, W. Kulig, A. Lamberg, C. Loison, A. Lyubartsev, M. S. Miettinen, et al., The Journal of Physical Chemistry B **119**, 15075 (2015).

[44] J. Seelig, Cell biology international reports **14**, 353360 (1990), URL http://dx.doi.org/10.1016/0309-1651(90)91204-H.

[45] A. A. Gurtovenko, M. Miettinen, , M. Karttunen, and I. Vattulainen, The Journal of Physical Chemistry B **109**, 21126 (2005).

[46] W. Zhao, A. A. Gurtovenko, I. Vattulainen, and M. Karttunen, The Journal of Physical Chemistry B **116**, 269 (2012).

[47] M. S. Miettinen, A. A. Gurtovenko, I. Vattulainen, and M. Karttunen, The Journal of Physical Chemistry B **113**, 9226 (2009).

[48] C. M. Franzin, P. M. Macdonald, A. Polozova, and F. M. Winnik, Biochimica et Biophysica Acta (BBA) - Biomembranes **1415**, 219 (1998).

[49] S. Ollila, M. T. Hyvönen, and I. Vattulainen, J. Phys. Chem. B **111**, 3139 (2007).

[50] O. H. S. Ollila, T. Ferreira, and D. Topgaard (2014), URL {http://dx.doi.org/10.5281/zenodo.13279}.

[51] T. P. Straatsma and H. J. C. Berendsen, The Journal of Chemical Physics **89** (1988).

[52] O. O. H. Samuli, *MD simulation trajectory and related files for POPC bilayer with 340mM NaCl (Berger model delivered by Tieleman, ffgmx ions, Gromacs 4.5)* (2015), URL http://dx.doi.org/10.5281/zenodo.32144.

[53] O. O. H. Samuli, *MD simulation trajectory and related files for POPC bilayer with 340mM CaCl_2 (Berger model delivered by Tieleman, ffgmx ions, Gromacs 4.5)* (2015), URL http://dx.doi.org/10.5281/zenodo.32173.

[54] S.-J. Marrink, O. Berger, P. Tieleman, and F. Jähnig, Biophysical Journal **74**, 931 (1998).

[55] J. Määttä (2015), URL {http://dx.doi.org/10.5281/zenodo.13934}.

[56] J. Mtt, *Dppc_berger_nacl* (2015), URL http://dx.doi.org/10.5281/zenodo.16319.

[57] J. Määttä, *Dppc_berger_nacl_1mol* (2015), URL http://dx.doi.org/10.5281/zenodo.17210.

[58] D. P. Tieleman, J. L. MacCallum, W. L. Ash, C. Kandt, Z. Xu, and L. Monticelli, J. Phys. Condens. Matter **18**, S1221 (2006).

[59] J. Määttä, *Dppc_berger_opls06* (2015), URL http://dx.doi.org/10.5281/zenodo.17237.

[60] J. Åqvist, The Journal of Physical Chemistry **94**, 8021 (1990).

[61] J. Määttä, *Dppc_berger_opls06_nacl* (2015), URL http://dx.doi.org/10.5281/zenodo.16484.

[62] J. Määttä, *Dppc_berger_opls06_nacl_1mol* (2016), URL http://dx.doi.org/10.5281/zenodo.46152.

[63] J. B. Klauda, R. M. Venable, J. A. Freites, J. W. O'Connor, D. J. Tobias, C. Mondragon-Ramirez, I. Vorobyov, A. D. M. Jr, and R. W. Pastor, J. Phys. Chem. B **114**, 7830 (2010).

[64] O. O. H. Samuli and M. Miettinen (2015), URL {http://dx.doi.org/10.5281/zenodo.13944}.

[65] R. M. Venable, Y. Luo, K. Gawrisch, B. Roux, and R. W. Pastor, The Journal of Physical Chemistry B **117**, 10183 (2013).

[66] S. Ollila, *MD simulation trajectory and related files for POPC bilayer with 350mM NaCl (CHARMM36, Gromacs 4.5)* (2015), URL http://dx.doi.org/10.5281/zenodo.32496.

[67] S. Ollila, *MD simulation trajectory and related files for POPC bilayer with 690mM NaCl (CHARMM36, Gromacs 4.5)* (2015), URL http://dx.doi.org/10.5281/zenodo.32497.

[68] S. Ollila, *MD simulation trajectory and related files for POPC bilayer with 950mM NaCl (CHARMM36, Gromacs 4.5)* (2015), URL http://dx.doi.org/10.5281/zenodo.32498.

[69] G. Mykhailo and O. O. H. Samuli, *Popc_charmm36_cacl2_035mol* (2015), URL http://dx.doi.org/10.5281/zenodo.35159.

[70] M. Javanainen, *POPC @ 310K, 450 mM of CaCl_2. Charmm36 with default Charmm ions* (2016), URL http://dx.doi.org/10.5281/zenodo.51185.

[71] G. Mykhailo and O. O. H. Samuli, *Popc_charmm36_cacl2_067mol* (2015), URL http://dx.doi.org/10.5281/zenodo.35160.

[72] G. Mykhailo and O. O. H. Samuli, *Popc_charmm36_cacl2_1mol* (2015), URL http://dx.doi.org/10.5281/zenodo.35156.

[73] J. Yoo, J. Wilson, and A. Aksimentiev, Biopolymers (2016).

[74] A. Maciejewski, M. Pasenkiewicz-Gierula, O. Cramariuc, I. Vattulainen, and T. Rog, The Journal of Physical Chemistry B **118**, 4571 (2014).

[75] M. Javanainen (2014), URL {http://dx.doi.org/10.5281/zenodo.13498}.

[76] M. Javanainen, *POPC @ 310K, varying amounts of NaCl. Model by Maciejewski and Rog* (2015), URL http://dx.doi.org/10.5281/zenodo.14976.

[77] O. H. S. Ollila, J. Mtt, and L. Monticelli, *MD simulation trajectory for POPC bilayer (Orange, Gromacs 4.5)* (2015), URL http://dx.doi.org/10.5281/zenodo.34488.

[78] O. H. S. Ollila, J. Mtt, and L. Monticelli, *MD simulation trajectory for POPC bilayer with 140mM NaCl (Orange, Gromacs 4.5)* (2015), URL http://dx.doi.org/10.5281/zenodo.34491.

[79] O. H. S. Ollila, J. Mtt, and L. Monticelli, *MD simulation trajectory for POPC bilayer with 510mM NaCl (Orange, Gromacs 4.5)* (2015), URL http://dx.doi.org/10.5281/zenodo.34490.

[80] S. Ollila, J. Mtt, and L. Monticelli, *MD simulation trajectory for POPC bilayer with 1000mM NaCl (Orange, Gromacs 4.5)* (2015), URL http://dx.doi.org/10.5281/zenodo.34497.

[81] O. H. S. Ollila, J. Mtt, and L. Monticelli, *MD simulation trajectory for POPC bilayer with 510mM CaCl_2 (Orange, Gromacs 4.5)* (2015), URL http://dx.doi.org/10.5281/zenodo.34498.

[82] J. P. M. Jämbeck and A. P. Lyubartsev, The Journal of Physical Chemistry B **116**, 3164 (2012).

[83] J. Määttä (2014), URL {http://dx.doi.org/10.5281/zenodo.13287}.

[84] D. Beglov and B. Roux, The Journal of Chemical Physics **100** (1994).

[85] B. Roux, Biophysical Journal **71**, 3177 (1996), ISSN 0006-3495, URL http://www.sciencedirect.com/science/article/pii/S0006349596795115.

[86] J. Melcr, *Simulation files for DPPC lipid membrane with Slipids force field for Gromacs MD simulation engine* (2016), URL http://dx.doi.org/10.5281/zenodo.55322.

[87] J. P. M. Jämbeck and A. P. Lyubartsev, Journal of Chemical Theory and Computation **8**, 2938 (2012).

[88] M. Javanainen, *Popc @ 310k, slipids force field.* (2015), dOI: 10.5281/zenodo.13887.

[89] D. E. Smith and L. X. Dang, The Journal of Chemical Physics **100** (1994).

[90] M. Javanainen, *POPC @ 310K, 130 mM of NaCl. Slipids with ions by Smith & Dang* (2015), URL http://dx.doi.org/10.5281/zenodo.35275.

[91] M. Javanainen, *POPC @ 310K, 450 mM of CaCl_2. Slipids with default Amber ions* (2016), URL http://dx.doi.org/10.5281/zenodo.51182.

[92] C. J. Dickson, B. D. Madej, . A. Skjevik, R. M. Betz, K. Teigen, I. R. Gould, and R. C. Walker, Journal of Chemical Theory and Computation **10**, 865 (2014).

[93] M. Girych and O. H. S. Ollila, *Popc_amber_lipid14_verlet* (2015), URL http://dx.doi.org/10.5281/zenodo.30898.

[94] M. Girych and O. H. S. Ollila, *Popc_amber_lipid14_nacl_015mol* (2015), URL http://dx.doi.org/10.5281/zenodo.30891.

[95] M. Girych and O. H. S. Ollila, *Popc_amber_lipid14_nacl_1mol* (2015), URL http://dx.doi.org/10.5281/zenodo.30865.

[96] G. Mykhailo and O. O. H. Samuli, *Popc_amber_lipid14_cacl2_035mol* (2015), URL http://dx.doi.org/10.5281/zenodo.34415.

[97] G. Mykhailo and O. O. H. Samuli, *Popc_amber_lipid14_cacl2_1mol* (2015), URL http://dx.doi.org/10.5281/zenodo.35074.

[98] J. P. Ulmschneider and M. B. Ulmschneider, Journal of Chemical Theory and Computation **5**, 1803 (2009).

[99] M. Girych and O. H. S. Ollila, *Popc_ulmschneider_opls_verlet_group* (2015), URL http://dx.doi.org/10.5281/zenodo.30904.

[100] M. Girych and O. H. S. Ollila, *Popc_ulmschneider_opls_nacl_015mol* (2015), URL http://dx.doi.org/10.5281/zenodo.30892.

[101] M. Girych and O. H. S. Ollila, *Popc_ulmschneider_opls_nacl_1mol* (2015), URL http://dx.doi.org/10.5281/zenodo.30894.

[102] H. Hauser, M. C. Phillips, B. Levine, and R. Williams, Nature **261**, 390 (1976).

[103] H. Hauser, W. Guyer, B. Levine, P. Skrabal, and R. Williams, Biochimica et Biophysica Acta (BBA) - Biomembranes **508**, 450 (1978), ISSN 0005-2736, URL http://www.sciencedirect.com/science/article/pii/0005273678900913.

[104] L. Herbette, C. Napolitano, and R. McDaniel, Biophysical Journal **46**, 677 (1984).

[105] B. Hess, C. Holm, and N. van der Vegt, The Journal of Chemical Physics **124** (2006).

[106] A. A. Chen, , and R. V. Pappu, The Journal of Physical Chemistry B **111**, 11884 (2007).

[107] M. M. Reif, M. Winger, and C. Oostenbrink, Journal of Chemical Theory and Computation **9**, 1247 (2013), pMID: 23418406, http://dx.doi.org/10.1021/ct300874c, URL http://dx.doi.org/10.1021/ct300874c.

[108] I. Leontyev and A. Stuchebrukhov, Phys. Chem. Chem. Phys. **13**, 2613 (2011).

[109] W. L. Jorgensen, D. S. Maxwell, and J. Tirado-Rives, Journal of the American Chemical Society **118**, 11225 (1996).

[110] M. Kohagen, P. E. Mason, and P. Jungwirth, The Journal of Physical Chemistry B **120**, 1454 (2016).

[111] M. Kohagen, P. E. Mason, and P. Jungwirth, The Journal of Physical Chemistry B **118**, 7902 (2014).

[112] A. Arkhipov, Y. Shan, R. Das, N. Endres, M. Eastwood, D. Wemmer, J. Kuriyan, and D. Shaw, Cell **152**, 557 (2013).

[113] K. Kaszuba, M. Grzybek, A. Orowski, R. Danne, T. Rg, K. Simons, . Coskun, and I. Vattulainen, Proceedings of the National Academy of Sciences **112**, 4334 (2015).

[114] M. S. Miettinen, *Molecular dynamics simulation trajectory of a fully hydrated DMPC lipid bilayer* (2013), URL http://dx.doi.org/10.5281/zenodo.51635.

[115] M. S. Miettinen, *Molecular dynamics simulation trajectory of a cationic lipid bilayer: 6/94 mol% DMTAP/DMPC* (2016), URL http://dx.doi.org/10.5281/zenodo.51639.

[116] M. S. Miettinen, *Molecular dynamics simulation trajectory of a cationic lipid bilayer: 50/50 mol% DMTAP/DMPC* (2016), URL http://dx.doi.org/10.5281/zenodo.51748.

[117] J. Määttä (2015), URL {http://dx.doi.org/10.5281/zenodo.16320}.

[118] J. Määttä, *Dppc_berger_nacl_1mol_scaled* (2015), URL http://dx.doi.org/10.5281/zenodo.17228.

[119] J. Määttä (2015), URL {http://dx.doi.org/10.5281/zenodo.16485}.

[120] J. Mtt, *Dppc_berger_opls06_nacl_1mol_scaled* (2015), URL http://dx.doi.org/10.5281/zenodo.17209.

[121] M. Javanainen, *POPC @ 310K, varying amounts of NaCl. Slipids with ECC-scaled ions* (2015), URL http://dx.doi.org/10.5281/zenodo.35193.

[122] M. Javanainen, *POPC @ 310K, 450 mM of CaCl_2. Charmm36 with ECC-scaled ions* (2016), URL http://dx.doi.org/10.5281/zenodo.45008.

[123] M. Javanainen, *POPC @ 310K, 450 mM of CaCl_2. Slipids with ECC-scaled ions* (2016), URL http://dx.doi.org/10.5281/zenodo.45007.

[124] J. Melcr, *Simulation files for POPC lipid membrane with Charmm36 force field without NBFIX for Gromacs MD simulation engine* (2016), URL http://dx.doi.org/10.5281/zenodo.55318.

[125] S. Pronk, S. Pll, R. Schulz, P. Larsson, P. Bjelkmar, R. Apostolov, M. R. Shirts, J. C. Smith, P. M. Kasson, D. van der Spoel, et al., Bioinformatics **29**, 845 (2013).

[126] M. J. Abraham, T. Murtola, R. Schulz, S. Pll, J. C. Smith, B. Hess, and E. Lindahl, SoftwareX **12**, 19 (2015), ISSN 2352-7110, URL http://www.sciencedirect.com/science/article/pii/S2352711015000059.

[127] J. C. Phillips, R. Braun, W. Wang, J. Gumbart, E. Tajkhorshid, E. Villa, C. Chipot, R. D. Skeel, L. Kalé, and K. Schulten, J. Comput. Chem. **26**, 1781 (2005).

[128] D. van der Spoel, E. Lindahl, B. Hess, A. R. van Buuren, E. Apol, P. J. Meulenhoff, D. P. Tieleman, A. L. T. M. Sijbers, K. A. Feenstra, R. van Drunen, et al., *GROMACS user manual version 4.0* (2005), URL www.gromacs.org.

[129] O. H. S. Ollila and et al. (2015), URL https://github.com/NMRLipids/lipid_ionINTERACTION.

[130] T. M. Ferreira, F. Coreta-Gomes, O. H. S. Ollila, M. J. Moreno, W. L. C. Vaz, and D. Topgaard, Phys. Chem. Chem. Phys. **15**, 1976 (2013).

[131] O. Berger, O. Edholm, and F. Jähnig, Biophys. J. **72**, 2002 (1997).

[132] M. Bachar, P. Brunelle, D. P. Tieleman, and A. Rauk, J. Phys. Chem. B **108**, 7170 (2004).

[133] B. Hess, H. Bekker, H. J. C. Berendsen, and J. G. E. M. Fraaije, J. Comput. Chem. **18**, 1463 (1997).

[134] B. Hess, Journal of Chemical Theory and Computation **4**, 116 (2008).

[135] T. Darden, D. York, and L. Pedersen, The Journal of Chemical Physics **98** (1993).

[136] U. L. Essman, M. L. Perera, M. L. Berkowitz, T. Larden, H. Lee, and L. G. Pedersen, J. Chem. Phys. **103**, 8577 (1995).

[137] G. Bussi, D. Donadio, and M. Parrinello, The Journal of Chemical Physics **126** (2007).

[138] M. Parrinello and A. Rahman, J. Appl. Phys. **52**, 7182 (1981).

[139] H. J. C. Berendsen, J. P. M. Postma, W. F. van Gunsteren, A. DiNola, and J. R. Haak, J. Chem. Phys. **81**, 3684 (1984).

[140] S. Nose, Mol. Phys. **52**, 255 (1984).

[141] W. G. Hoover, Phys. Rev. A **31**, 1695 (1985).

[142] J. Lee, X. Cheng, J. M. Swails, M. S. Yeom, P. K. Eastman, J. A. Lemkul, S. Wei, J. Buckner, J. C. Jeong, Y. Qi, et al., Journal of Chemical Theory and Computation **0**, null (0).

[143] S. Pll and B. Hess, Computer Physics Communications **184**, 2641 (2013), ISSN 0010-4655, URL http://www.sciencedirect.com/science/article/pii/S0010465513001975.

[144] L. Martínez, R. Andrade, E. G. Birgin, and J. M. Martínez, J. Comput. Chem. **30**, 2157 (2009).

[145] W. Humphrey, A. Dalke, and K. Schulten, Journal of Molecular Graphics **14**, 33 (1996).

[146] M. Abraham, D. van der Spoel, E. Lindahl, B. Hess, and the GROMACS development team, *GROMACS user manual version 5.0.7* (2015), URL www.gromacs.org.

[147] W. L. Jorgensen, J. D. Madura, and C. J. Swenson, Journal of the American Chemical Society **106**, 6638 (1984).

[148] W. L. Jorgensen and J. Gao, The Journal of Physical Chemistry **90**, 2174 (1986).

[149] W. L. Jorgensen, The Journal of Physical Chemistry **90**, 1276 (1986).

[150] W. L. Jorgensen and J. Tirado-Rives, Journal of the American Chemical Society **110**, 1657 (1988).

[151] J. M. Briggs, T. B. Nguyen, and W. L. Jorgensen, The Journal of Physical Chemistry **95**, 3315 (1991).

[152] W. L. Jorgensen, J. Chandrasekhar, J. D. Madura, R. W. Impey, and M. L. Klein, The Journal of Chemical Physics **79** (1983).

[153] O. H. S. Ollila and M. Retegan, *Md simulation trajectory and related files for popc bilayer (lipid14, gromacs 4.5)* (2014), URL `http://dx.doi.org/10.5281/zenodo.12767`.

[154] J. Domaski, P. Stansfeld, M. Sansom, and O. Beckstein, The Journal of Membrane Biology **236**, 255 (2010), ISSN 0022-2631.